

Integrative Machine Learning Approach for Identification of new molecular scaffold and Prediction of Inhibition Responses in Cancer Cells Using Multi-Omics Data

Aman Chandra Kaushik^a, Shubham Krushna Talware^a, Mohammad Imran Siddiqi^a

^aDivision of Biochemistry and Structural Biology, CSIR-Central Drug Research Institute, Jankipuram Extension, Sitapur Road, Lucknow, Uttar Pradesh, 226031, India.

Corresponding Author: Mohammad Imran Siddiqi mi_siddiqi@cdri.res.in

MATERIALS AND METHODS

Drug screening from single-cell RNA-Seq data:

For single-cell RNA sequencing, the cancer cell lines were dissociated into single cells, and the single cells were captured and sequenced using standard protocols. The sequencing data was processed using the Cell Ranger pipeline to generate gene expression data. All scRNA-sequencing, drug sensitivity, and other cell line data are available on the Figshare Dataset. The single-cell data was analyzed using R packages, including Seurat, to identify cell types and to compare the transcriptional responses to drug perturbations. Finally, the cancer cell lines were used for in vitro drug screening, and the data on drug response was combined with data from RNA sequencing and single-cell RNA sequencing in order to computationally predict drug responses. These data were also used to explore the heterogeneity of drug response and cell line composition.

To identify the genes that were differentially expressed in response to Idasanutlin treatment, a differential expression analysis was performed (Figure S3). The volcano plot displayed a strong upregulation of TP53 effector pathway genes in TP53 wild-type cell lines. This effect was particularly evident in the volcano plot depicting the gene expression changes across TP53 wild-type cell lines in response to Idasanutlin treatment (Figure S3). For this and subsequent differential expression studies, effect size estimates and p-values were calculated. To illustrate the average log-fold change estimates for the top differentially expressed genes in each cell line, a heatmap was created. (Figure S3). In contrast, TP53 mutant cell lines showed very minor alterations in gene expression in response to Idasanutlin therapy, as depicted in Figure S3.

Similarities search for Tumour suppressor p53/oncoprotein MDM2 analysis using Machine Learning

First, we converted the datatype of standard value from "object" to "float", then kept only entries with the standard unit (nM), followed by deleting duplicate molecules. Further, we labeled those compounds having IC₅₀ values of less than 1000 nM were referred as active; while those greater than 10,000 nM were referred to as inactive, and those with values between 1,000 and 10,000 nM were considered as intermediate respectively, for further evaluations. Then we did a Lipinski calculation to evaluate the drug-likeness of compounds, which is based on the pharmacokinetic profile or Absorption, Distribution, Metabolism, and Excretion (ADME). We found the total number of compounds in the unfiltered data set (1224), the total number of compounds in the filtered data set (440), and the total number of compounds not compliant with the Rule of five (784). The detailed analysis is shown in Figure S4. We also did PAINS (Pan Assay Interference Compounds) analysis and obtained 7 compounds identified as PAINS and 443 compounds as non-PAINS.

We did statistical analysis for the dataset of compounds that fulfilled the rule of five, where the mean of molecular weight was 480.733 while the standard deviation was 65.692, for hydrogen bond acceptors -the mean was 4.500 and the standard deviation was 2.110, similarly for hydrogen bond donor - mean was 1.086 and standard deviation was 0.884 and for logP value - mean was 5.129 and standard deviation was 0.899. We also did calculations for those who violated the rule of five. The mean of molecular weight was 596.724 while the standard deviation was 139.053, the number of hydrogen bond acceptors (mean 5.272 and standard deviation was 2.441), the number of hydrogen bond donors (mean 1.246 and standard deviation 2.329) and logP value was (mean 6.228 and standard deviation 1.168).

Then, we calculated MACCS and Morgan fingerprints for all compounds including controls. Tanimoto similarity and distance matrix were calculated for all compounds with respect to Idasanutlin. The clustering was performed for all compounds with respect to Idasanutlin. The resulting clusters were observed based on Tanimoto similarity and explained below.

Molecular Dynamics Simulation Study

The system was built in an orthorhombic simulation box using the simple point charge water (SPC) model and periodic boundary conditions (PBC). The neutralization of the generated system was achieved by incorporating counter ions and adjusting the SPC molecules' geometry in the system. The SHAKE algorithm was used for neutralizing bond lengths of the

heavy atom involving hydrogens, while electrostatic interactions were incorporated using the particle mesh Ewald (PME) method.

The simulation protocol comprised of several steps. Initially, the system, comprising the MDM2 structure with the top 13 compounds (compound A to compound M), was minimized by the steepest descent method with restraints on the solute for a maximum of 2,000 iterations. This was followed by the conjugate gradient method with a threshold energy of 50 Kcal/mol/Å. To establish equilibrium, a 10 picosecond (ps) simulation was executed at a temperature of 10K, on the non-hydrogen solute atoms in the NVT ensemble. Subsequently, a 100 ps MD simulation was conducted with restraints on the non-hydrogen solute atoms in the NPT ensemble at 10K temperature. Likewise, a 24 ps simulation was executed, allowing the system to relax devoid of restraints at 300K temperature in the NPT ensemble. Trajectories were recorded at intervals of 2.8 ps, with an energy recording interval of 1.2 ps.

RESULTS

Variant allele frequencies of the Ovarian Cancer

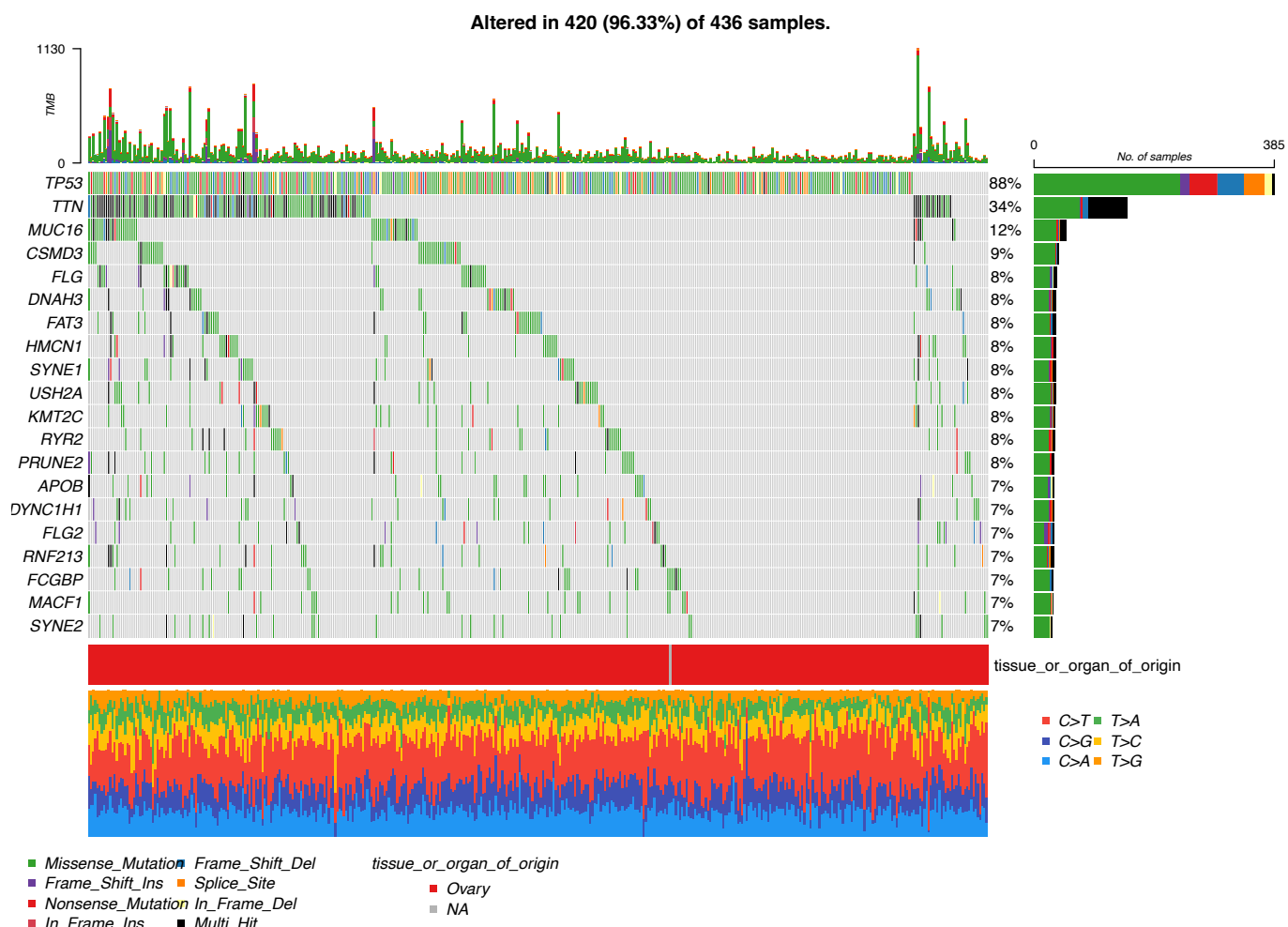


Figure S1: Mutational landscape of ovarian cancer. Bar plot of the mutations among 420 patients with ovarian cancer. The top 20 frequently mutated genes are listed and their frequency.

TP53 : [Somatic Mutation Rate: 88.3%]
NM_000546

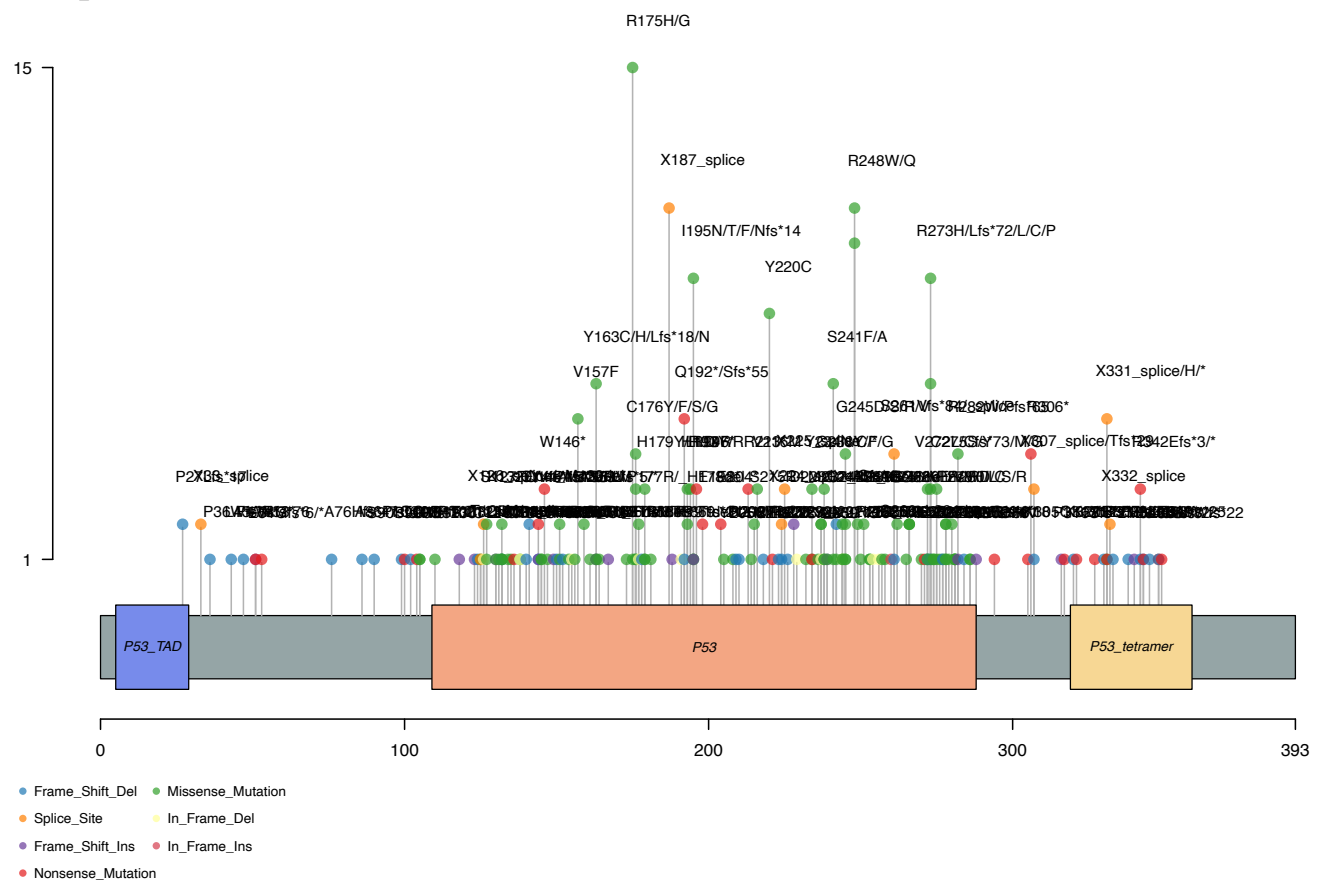


Figure S2: Mutational pattern of *TP53* in Ovarian cancer. Lollipop plot displaying the mutational pattern of *TP53* in Ovarian cancer.

Single-cell expression profiles

The PCA and UMAP analyses were carried out to explore the transcriptional response profiles of cell lines to varying treatment conditions. PCA was done on the log fold change profiles of 5000 genes with the maximum across-cell-line variance, with each gene mean-centered. Only cell lines with at least 10 cells in both the control and treatment conditions were included. The UMAP method, as implemented in the "Seurat" package, was then utilized to estimate the embedding of transcriptional response profiles. Response profiles were restricted to those with at least 10 cells per condition and at most 40 cells in total. The top 25 PCs were computed from the 5000 genes with the maximum variance across the selected profiles. UMAP was then run in this PC space, using cosine distance between samples, with an "n.neighbors" parameter of 15 and "min.dist" of 0.7. This investigation provided insights into the

transcriptional response of cell lines against different treatment conditions and identified potential biomarkers of drug response.

For cell cycle analysis, the authors utilized the Seurat function CellCycleScoring, which employs gene lists specific to the S and G2M phases to classify cell cycle stages. An R function was used to evaluate how the proportion of cells in each phase varied under treatment and control conditions for each cell line. Aggregate scores, which depicted how each compound altered the cell cycle's composition, were calculated using weighted averages across cell lines based on variations in the proportion of cells in each phase. The measured drug sensitivity of the cell lines was used to calculate the weights, bounded between 0 and 1.

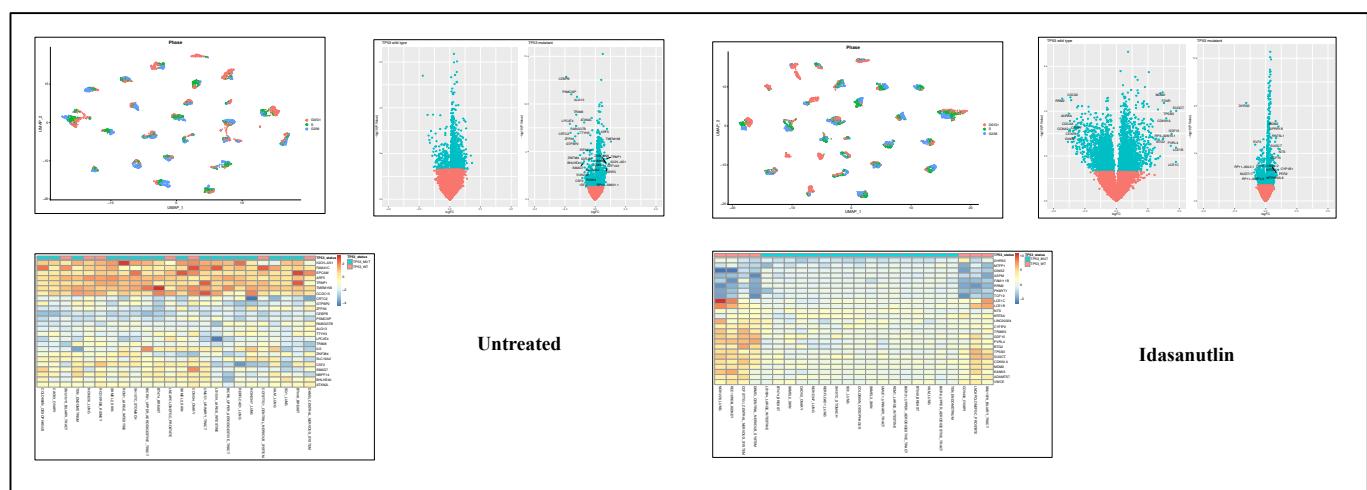


Figure S3: Untreated: **A.** Quantification of DMSO impact on cell-cycle phase. The transcriptional variability in the cell lines containing the TP53 mutation is shown by UMAP embedding by the cell-cycle phase. **B.** Differential expression analysis revealing the up-regulated/down-regulated genes in response to DMSO control. Volcano plot depicting significantly up-regulated genes of the TP53 effector pathway in the TP53 wild-type cell lines, demonstrating significant alterations in gene expression across TP53 WT cell lines in response to DMSO control. **C.** Heatmap of the top differentially expressed genes for each cell line, with average log fold-change estimations. In line with TP53 mutant cell lines, exhibiting little change in gene expression in response to DMSO control.

Idasanutlin: **A.** Quantification of Idasanutlin impact on cell-cycle phase. The transcriptional variability in the cell lines containing the TP53 mutation is shown by UMAP embedding by the cell-cycle phase. **B.** Differential expression analysis revealing the up-regulated/down-

regulated genes in response to Idasanutlin treatment. Volcano plot depicting significantly up-regulated genes of the TP53 effector pathway in the TP53 wild-type cell lines, demonstrating significant alterations in gene expression across TP53 WT cell lines in response to Idasanutlin treatment. C. Heatmap of the top differentially expressed genes for each cell line, with average log fold-change estimations. The sensitivity of Idasanutlin is given by area under the curve (AUC), in line with TP53 mutant cell lines, exhibiting little change in gene expression in response to Idasanutlin treatment.

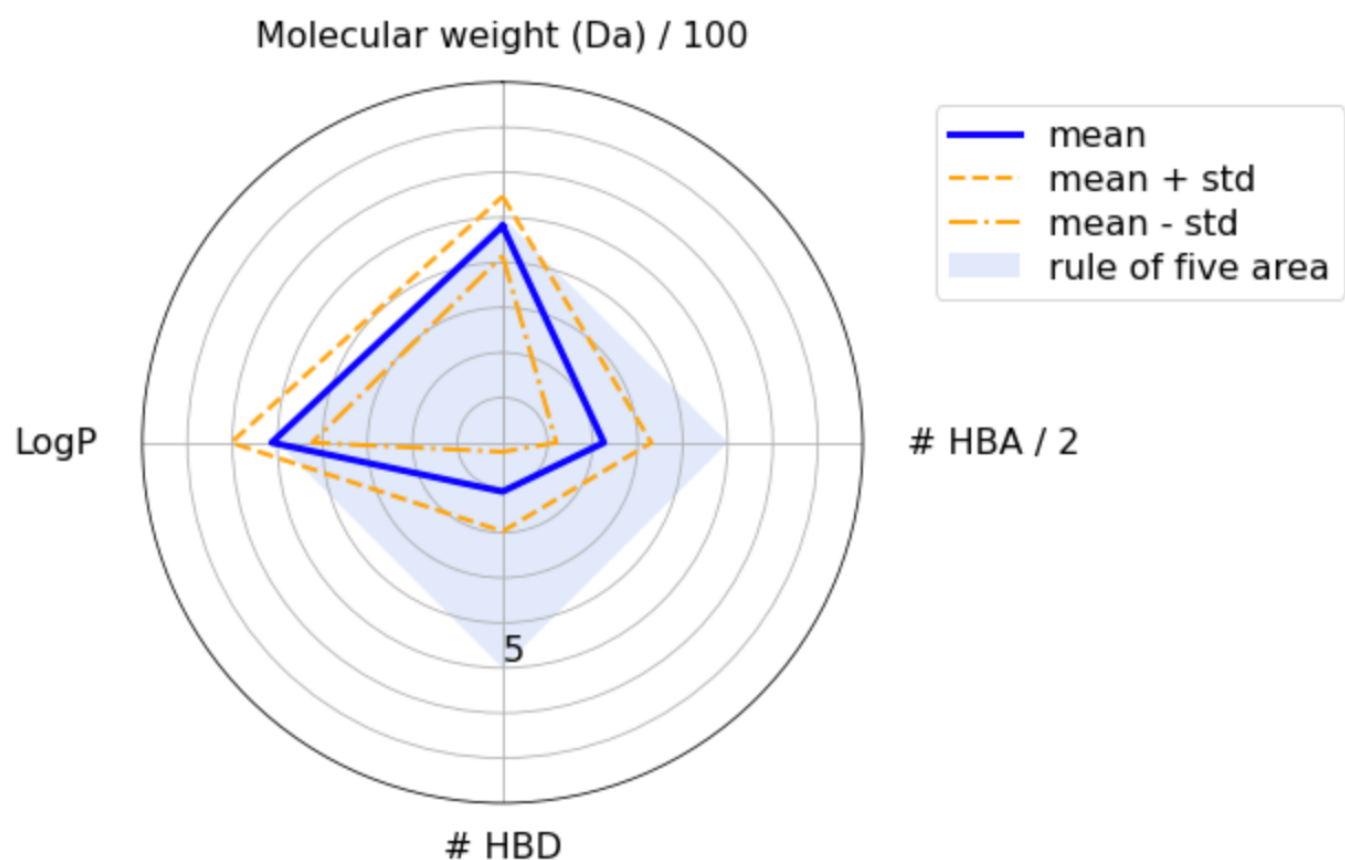


Figure S4: Radar plot for the dataset of compounds that fulfill the Rule of five

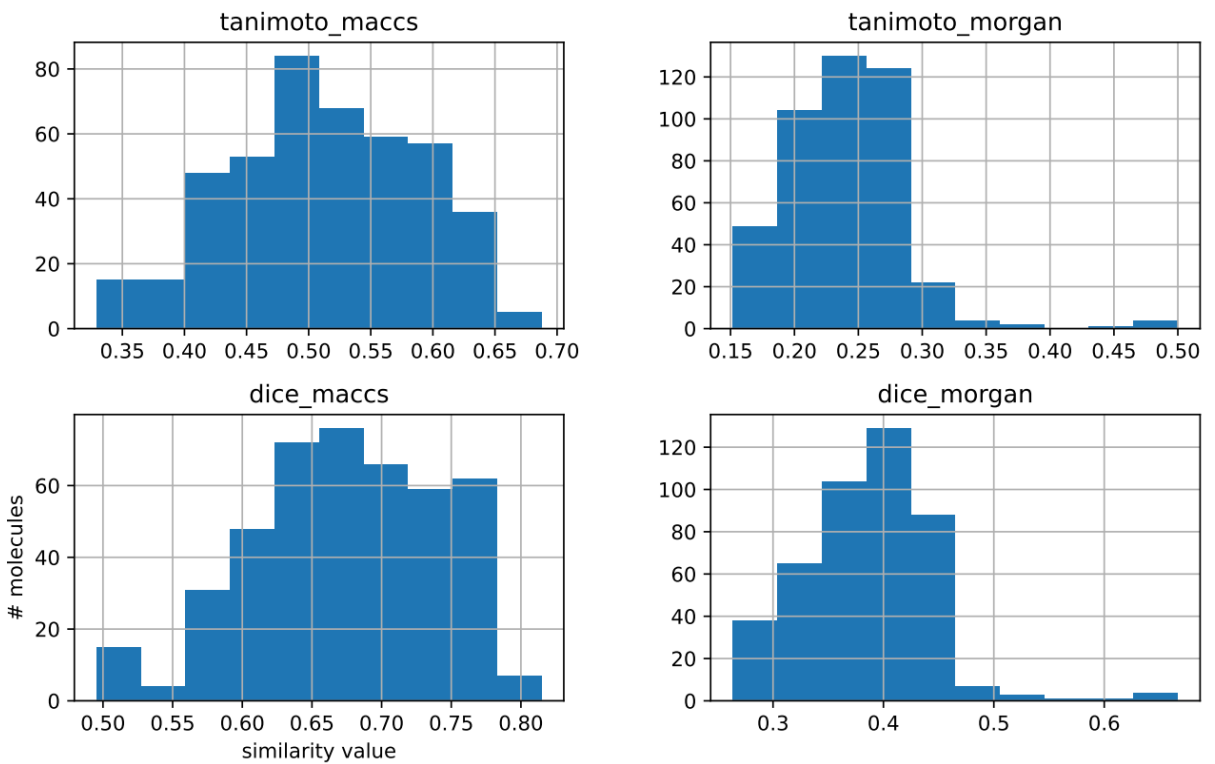


Figure S5: Distribution of similarity values for query molecule (Idasanutlin) and all molecules using MACCS and Morgan.

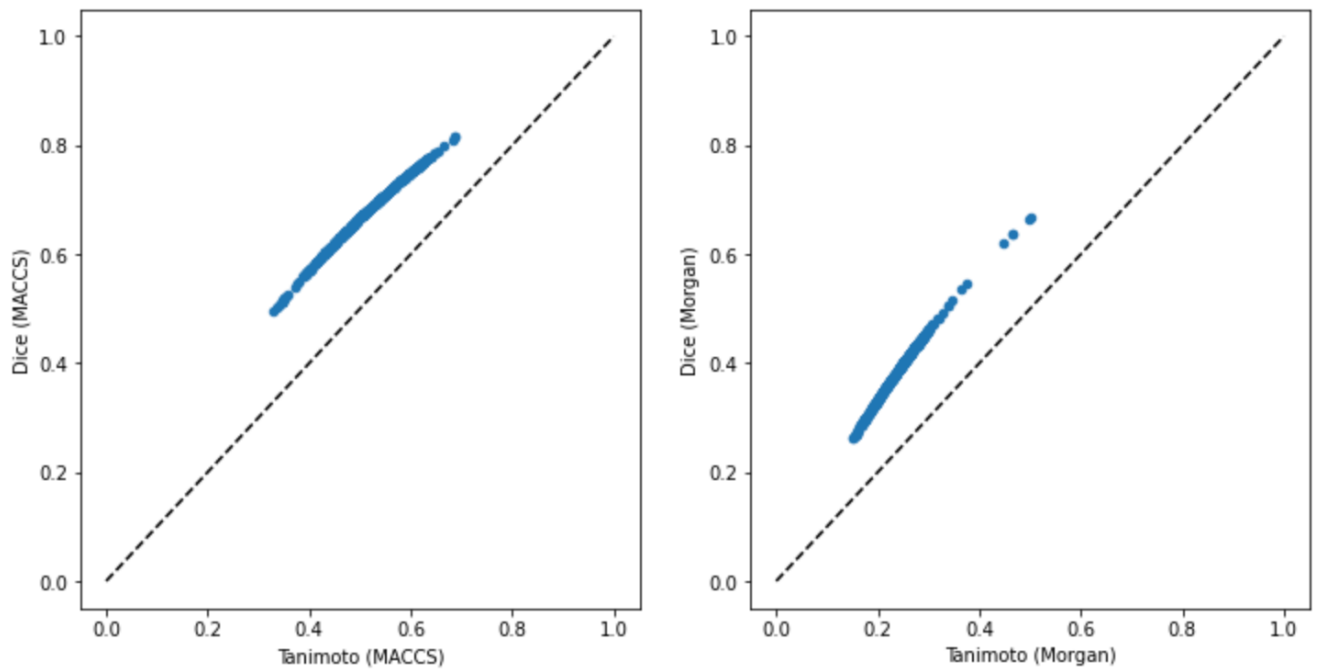


Figure S6: Comparative analysis between Tanimoto and Dice similarities for the two fingerprints

Clustering of the molecules based on their fingerprint similarity

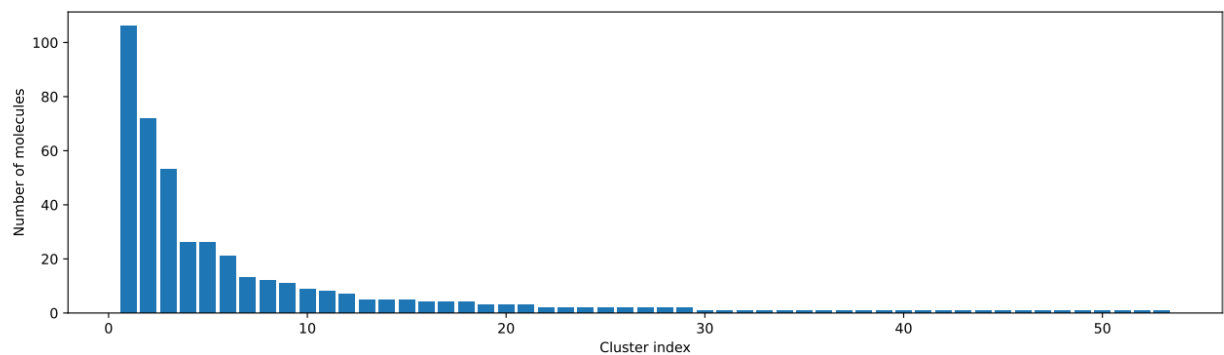


Figure S7: Plot of the clusters: clustering of the molecules based on their fingerprint similarity

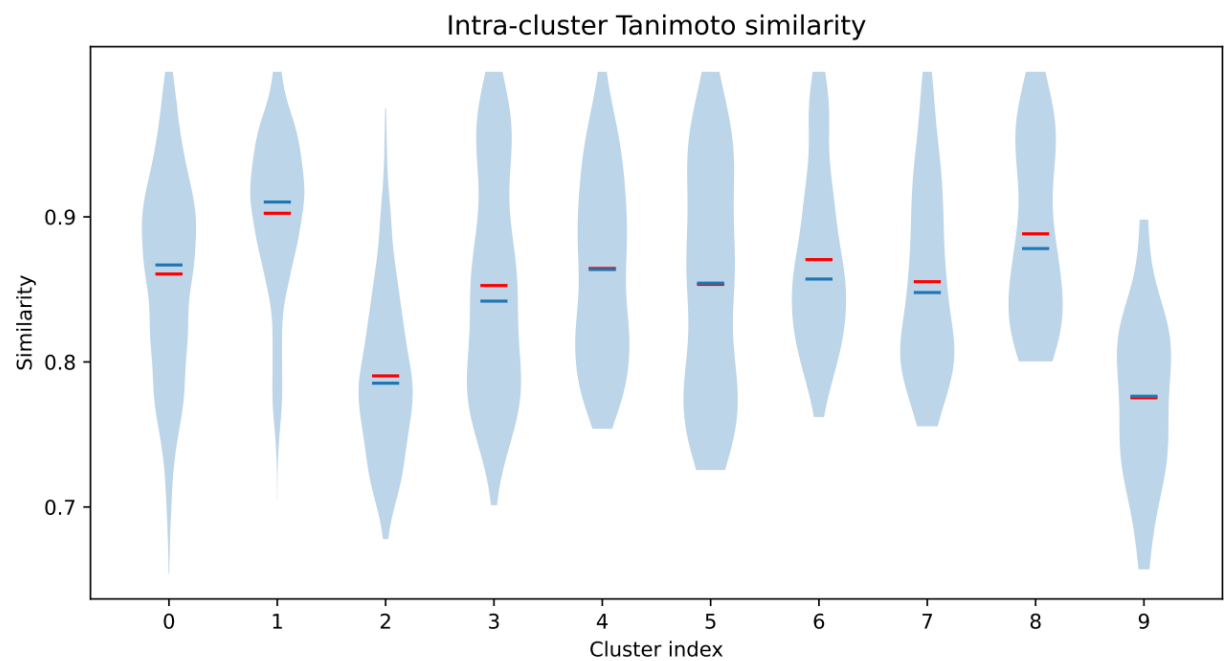


Figure S8: Similarity between two fingerprints or clusters using tanimoto similarities where similarity metrics were compared based on their ranking of the compounds

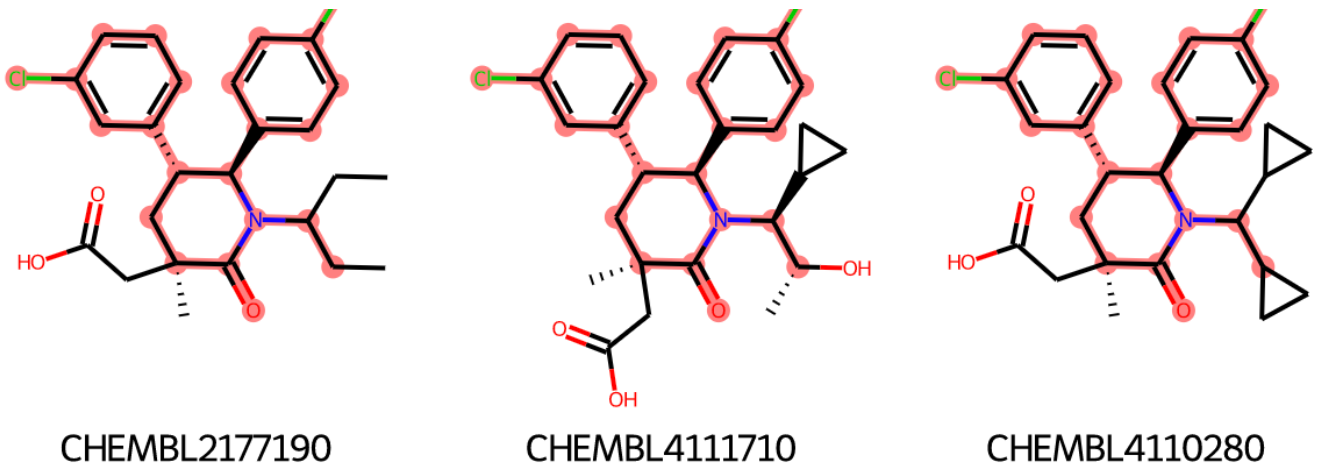


Figure S9: Calculation of maximum common substructure using FMCS algorithm

Molecular Docking Analysis

Our machine learning was established on RG-7388 (Idasanutlin), based upon which we have retrieved the 80 molecules from the CHEMBL database using a machine learning based similarity search approach. Hence we also docked Idasanutlin (Compound A) into the pocket of AM-8553 (bound ligand, PDB ID: 4ERF). The docking score for which was -6.406, and the interactions reported were: i.e. Pi-pi stacking and hydrogen bonding interaction with Hie96 and salt bridge with Lys94. It has been observed that the interactions were conserved with respect to AM-8553. AM-8553 had shown a docking score of -9.635 which is shown in Figure S10. Moreover, these interactions around the MDM2 site were noted in all 11 compounds. Compound G has shown additional hydrogen bonding of the Cl atom with Hie96. Five compounds have shown an extra hydrogen bond with Lys94, named: Compounds B, C, D, E, I, and L, while preserving the AM-8553 interactions. Compound I has shown a unique hydrogen bond with Gly58, along with other interactions mentioned above.

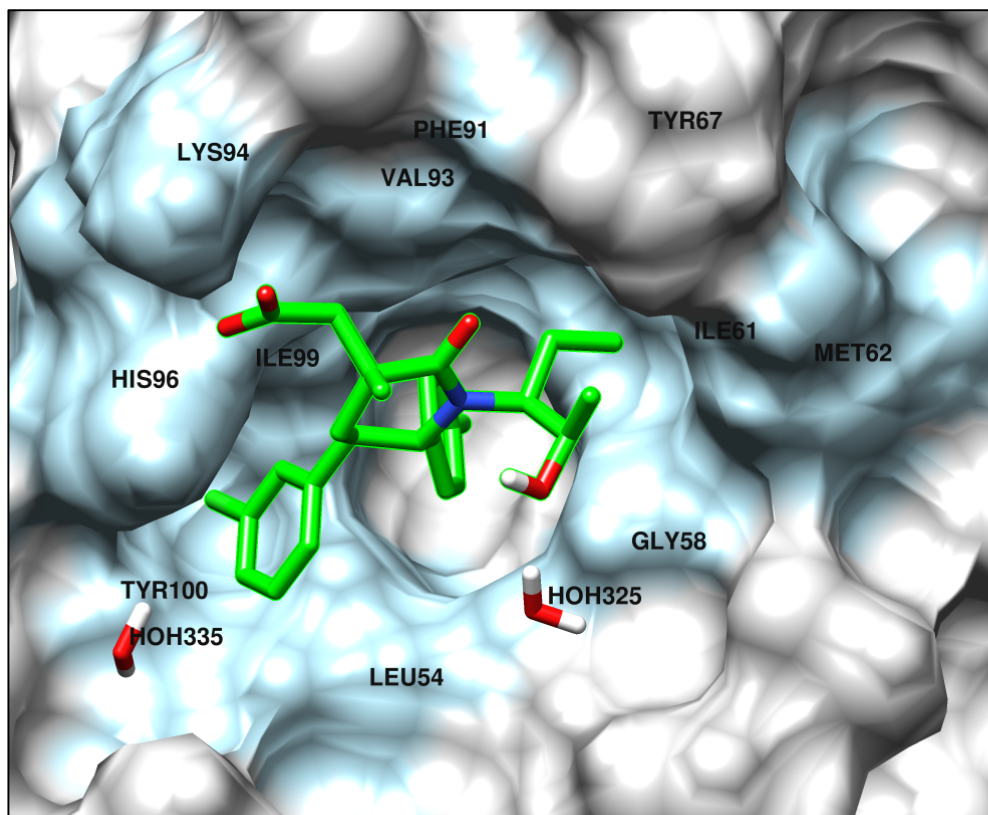


Figure S10: Docking pose of reference compound (AM-8553) around the p53 binding domain. The reported docking score was -9.635.

Molecular Dynamics Simulation Analysis

The ligand torsions plot provides a comprehensive overview of the conformational evolution of all compounds along with controls throughout the simulation trajectory. The plot consists of a top panel showing a 2D schematic of the ligand, with rotatable bonds color-coded for easy identification. Each rotatable bond torsion is represented by a dial plot, where the conformational changes over time are visually displayed. Additionally, bar plots of the same color summarize the data from the dial plots, presenting the probability density of each torsion.

DISCUSSION

Understanding the transcriptional effects of drugs on cancer cells is crucial in identifying their potential clinical application and molecular mechanisms. In this study, researchers identified a robust response in TP53 cell lines, suggesting that Idasanutlin may be a promising candidate for cancer therapy. Furthermore, the study highlighted the importance of

understanding mutational effects in different cancers pertaining to the prostate, ovary, and kidney. Machine learning and the integration of single-cell RNA-sequencing (scRNA-seq) and RNA-Seq data are emerging as promising avenues for predicting drug responses in cancer cells and enhancing cancer therapy. These techniques allow for a more comprehensive understanding of the molecular alterations associated with cancer, making it possible to identify potential drugs for mutated cancer.

The scRNA-seq analysis showed that Idasanutlin exhibited greater efficacy in the case of both mutated and wild-type cell lines by down-regulating effector pathway genes of TP53 along with targeting different phases of cell growth. The next task was to find druggable ovarian cancer targets that would pave the way for new treatments while influencing the TP53 pathway. Identifying therapeutic targets through the analysis of multiple-omics data can also aid in developing novel and more effective treatments for ovarian cancer patients.

In the MD simulation part of our article, we present important findings related to the conformational evolution of the 11 compounds along with controls throughout the simulation trajectory (0.0 to 100 ns for each complex). The ligand torsions plot of 11 compounds, along with controls, also incorporates information on the potential energy of the rotatable bonds, this is represented by the left Y-axis of the chart, where the values of the potential energy are shown alongside the histogram (Figure S11). The relationship between the torsional potential and the histogram provides information on the conformational strain experienced by the ligand in maintaining a bound conformation with the protein.

Furthermore, Figure S12 summarizes various characteristics of the 11 screened compounds along with controls. Among these parameters, the ligand RMSD indicates the ligand's root mean square deviation compared to the reference, usually the first frame of the simulation ($t=0$). The Radius of Gyration (rGyr) computes the "extendedness" of the ligand and corresponds to its principal moment of inertia. IntraHB represents the number of internal hydrogen bonds within the ligand molecule.

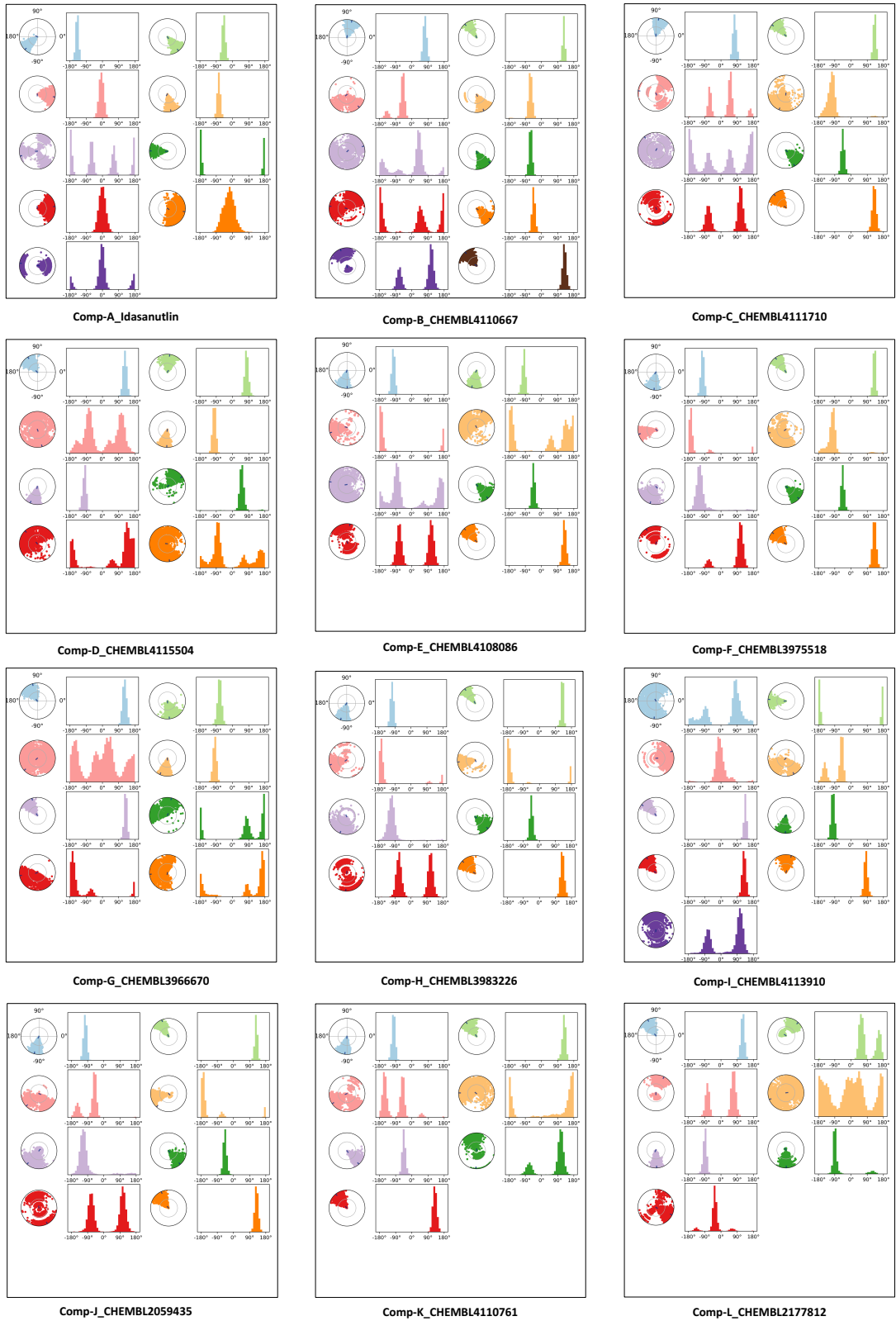


Figure S11: Ligand torsion plots summarizing the conformation evolutionary changes in the screened compounds throughout the simulation trajectory.



Figure S12: Plots summarizing various ligand properties including the RMSD, rGyr - Radius of Gyration, SASA - Solvent Accessible Surface Area, PSA – Polar Surface Area, IntraHB - Intramolecular Hydrogen Bonds, and MolSA - Molecular Surface Area, for the screened compounds.

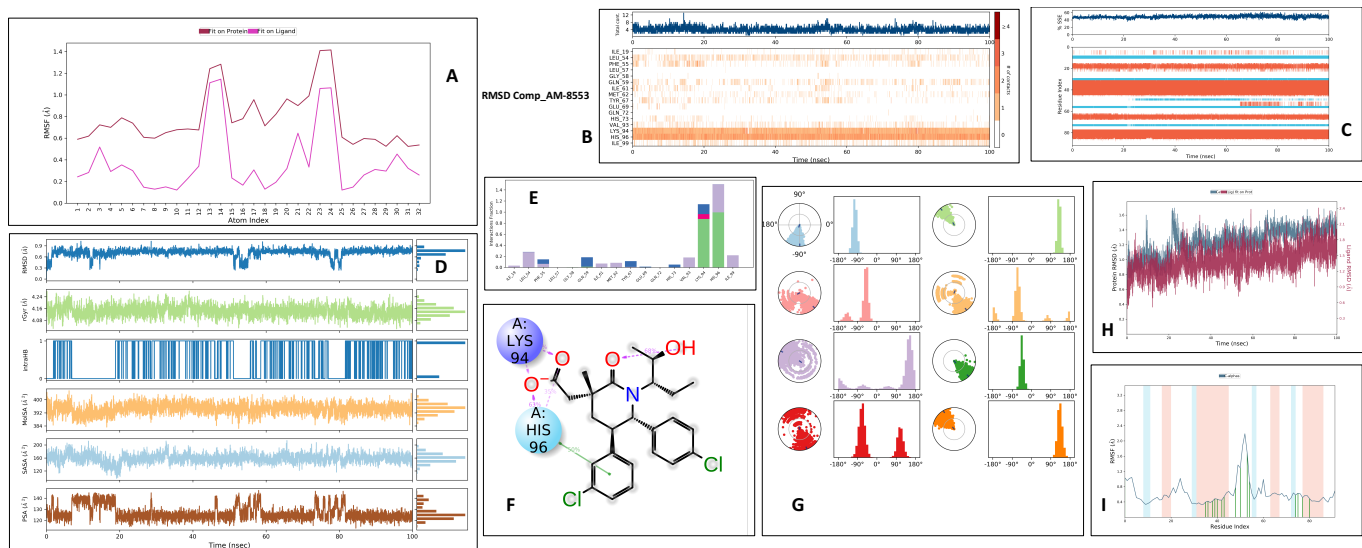


Figure S13: Figure showing all the compiled analysis for AM-8553 (reference compound).

(A) RMSF plot fit on the ligand of AM-8553-complex, **(B)** The interaction analysis during MD simulation, **(C)** depicts the SSE of AM-8553-complex, **(D)** depicts the PSA, SASA, MolSA, Intramolecular hydrogen bond interactions, Radius of gyration and RMSD of AM-8553-complex, **(E)** depicts interaction fraction, **(F)** depicts the ligand interaction diagram after MD simulation of AM-8553-complex, **(G)** depicts the torsion angle analysis of AM-8553-complex, **(H)** depicts the RMSD of AM-8553-complex ranged between 1.2 and 1.7 Å, not indicating any structural deviations. **(I)** Depicts the RMSF of AM-8553-complex ranged from 0.6 to 1.5 Å.